Int J Adv Manuf Technol (2017) 90:1351–1363
DOI 10.1007/s00170-016-9440-4

ORIGINAL ARTICLE

An investigation into the inhomogeneity of the microstructure and mechanical properties of explosive welded H62-brass/Q235B-steel clad plates

Qing-Lin Bai[1] · Lin-Jie Zhang[1] · Miao-Xia Xie[2] · Han-Xin Yang[3] · Jian-Xun Zhang[1]

Received: 1 August 2016 / Accepted: 4 September 2016 / Published online: 22 September 2016
© Springer-Verlag London 2016

Abstract Owing to excellent corrosion resistance, antifriction property, and economic efficiency, H62/Q235B explosive clad plates have been widely used in various fields. Therefore, detailed and systematic study into the microstructure and mechanical properties of this clad material is necessary. In this paper, the composition, microstructure, and mechanical properties of H62/Q235B explosive clad plates were analyzed by optical metallographic observation, mechanical tests, scanning electron microscope (SEM) observation, and energy dispersive spectrometer (EDS) analysis. The results showed that the bonding interface of this clad plate was periodical wavy, and the interface was bonded in two ways, one through wide transition layer with a width up to 280 μm while the other by narrow transition layer with a width less than 20 μm. The major structural components in the transition layer were supersaturated solid solutions. The microhardness of the transition layer was higher than that of base metals, and the microhardness of the base plates in the region near the bonding interface was affected by both force and heat. The shear strength of the H62/Q235B clad plate showed an obvious characteristic of anisotropy. Furthermore, the clad plate tended to crack along the transition layer when it was stretched because of the discontinuity of plastic deformation across H62/Q235B interface.

✉ Lin-Jie Zhang
zhanglinjie@mail.xjtu.edu.cn

[1] State Key Laboratory of Mechanical Behavior for Materials, Xi'an Jiaotong University, Xi'an 710049, China

[2] School of Mechanical and Electrical Engineering, Xi'an University of Architecture and Technology, Xi'an 710055, China

[3] Baoji Titanium Industry Group Clad Metal Plate Co., Ltd., Baoji, Shaanxi 721014, China

Keywords H62/Q235B clad plate · Explosive welding · Microstructure · Mechanical property · Inhomogeneity

1 Introduction

With the continuous development of industrial technologies, single metal materials struggle to meet the requirements of various production and applications for higher performance [1]. Clad plates which consist of dissimilar metal components can not only make use of the physical and chemical properties of two component materials, but also reduce the amount of precious metals used [2]. They show a dual advantage of high performance and low cost, therefore have been extensively applied in various fields, such as petrifaction, electric, transportation, nuclear energy, etc. [3]. Explosive cladding is a processing method for bonding heterogeneous metal plates. Based on the impact effect and high energy released by the high-speed detonation of explosives, the bonding surfaces of metal materials to be welded are collided, thus leading to severe plastic deformation and localized melting. As a result, a thin metallurgical bonding layer is formed [4–10]. This method shows strong applicability to materials, strong bonding strength, and favorable cycling processability [11]. In addition to these, it also presents high efficiency and capacity of welding large-area clad plates once, for which the method has been widely applied in the production and processing of clad plates [12, 13].

Copper and copper alloy present favorable corrosion resistance, antifriction property, and thermal conductivity as well as excellent vibration resistance and ability to resist impact loads [14]. Although having so many advantages, the difficulties in welding due to the special characteristics such as high heat conductivity, great expansion factor, and large solidification shrinkage percentage restrict the application of copper

Table 1 Chemical composition of H62-brass

Material	Cu	Fe	Pb	Sb	P	Others	Zn
ω_t/%	60.5 ~ 63.5	≤0.15	≤0.08	≤0.005	≤0.01	≤0.5	Balance

and copper alloy [15]. In order to obtain excellent welding joints, various welding methods are adopted, such as arc welding, ultrasonic welding [16, 17], laser welding [18–20], laser-arc hybrid welding [21], cold pressure welding [22], braze welding, electron beam welding [23, 24], and friction stir welding [25–28]. Characterized by the advantages of copper and copper alloy, much attention has been paid to the researches and applications of the exploded metal clad plates which use them as the flyer plates. Mróz et al. [29] analyzed the properties of the explosive welded Al/Cu bimetallic bars, and they found that the microhardness of the fused intermediate layer was much higher than those of the Al layer and the Cu layer. Durgutlu et al. [30] researched the bonding abilities of copper and steel with explosive welding using different welding parameters, and they found that wavy interfaces were more likely obtained in case of using higher explosive ratio and wider stand-off distance. Xue et al. [31] studied the explosive cladding technology of large-area copper-steel clad plates using numerical simulation. They obtained that the bonding rate of clad plates could reach up to about 100 % under reasonable plate thickness, charge quantity, and gap. And the mechanical properties of these clad plates met the requirements. Based on proper technological parameters, Zhai et al. [32] explosively welded B30 cupronickel and Q345A steel and studied the mechanical properties and microstructure. Results showed that the tensile strength and the shear strength of this clad plate reached to 483 and 222 MPa, separately; thus, it presented excellent microstructure and mechanical properties. Bian et al. [33] explored the feasibility of explosive cladding for copper and high-nitrogen steel through numerical simulation and experimental study and obtained the optimal technological parameters. Through numerical simulation on the temperature fields in the bonding zone of copper/iron explosive clad plates, Qu et al. [34] investigated the melting rate of metals at the

Table 2 Chemical composition of Q235B-steel

Material	C	Si	Mn	S	P	Cr	Ni	Fe
ω_t/%	≤0.2	≤0.35	≤0.7	≤0.045	≤0.045	≤0.03	≤0.03	Balance

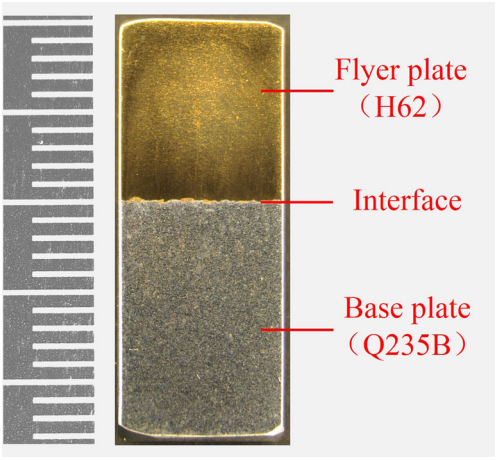

Fig. 1 Cross section of metallographic specimen of H62/Q235B clad plate

bonding surface of Cu/Fe composite plate jointed by explosive welding.

H62/Q235B clad plates have been widely utilized in various fields, including electric, metallurgy, machinery, nuclear energy, transportation, and defense industry owing to their excellent corrosion protection, abrasion resistance, machining property, electrical/thermal conductivities, and low cost. By means of studies, Li et al. [35] obtained the reasonable technology for producing H64/Q235B kelmet boards through explosive cladding. Liu et al. [36] intensively studied the bonding mechanism of H62/Q235B explosive clad plates. Taking H62/Q235B explosive clad plate as the material, this study investigated the morphology, microstructure, component distribution, and mechanical properties of the bonding interface. Compared with previous studies, the submitted work focused more on the inhomogeneity of both mechanical properties and microstructure of the H62-brass/Q235B-steel clad plates. The H62-brass/

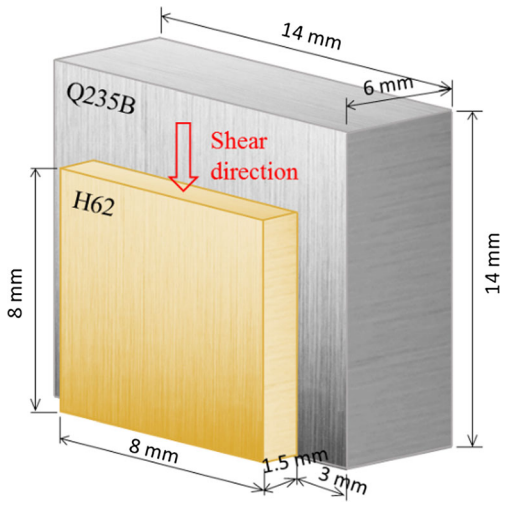

Fig. 2 Schematic of shear test specimen of H62/Q235B clad plate

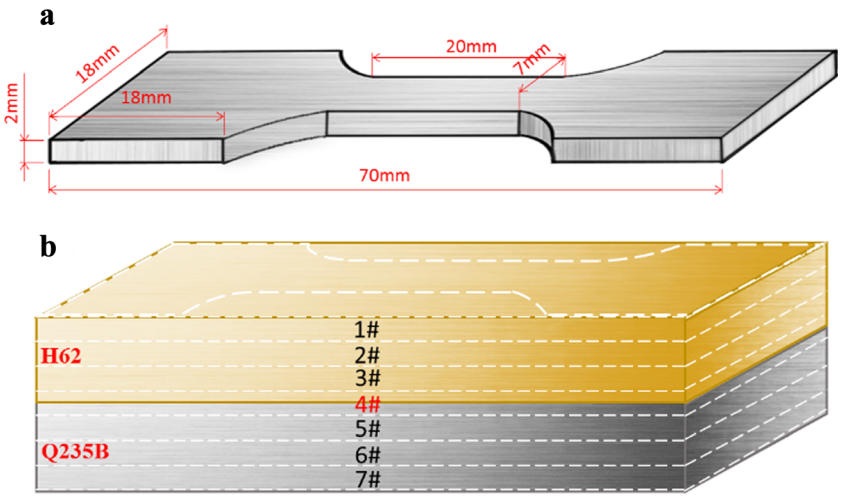

Fig. 3 Schematic of the specimen size and the sampling plan of the stratified tensile test

Q235B-steel clad plates discussed in this work would be used to manufacture chemical vessels and devices and therefore would be subjected to multiple bending process. The deformation and strain rate of clad plates would be highly heterogeneous during bending process and this might be beneficial to local shear failure. In order to minimize the risk of local failure, mastering the detailed information about the inhomogeneity of the mechanical properties of H62-brass/Q235B-steel clad plates is of great importance. So the aim of this work is to lay the foundation for controlling the incompatible deformation in the subsequent machining process (bending, reelpipe, etc.) of this clad plate and provide data for the optimization of these processing technologies.

2 Experimental materials and methods

2.1 Experimental materials

The clad plate studied in this study was composed of H62-brass (Table 1) as the flyer plate and Q235B-steel (Table 2) as the base plate. After explosive cladding, the generated plate was 24.5 mm in total thickness. Thereinto, the flyer plate and base plate were 10 and 14.5 mm thick, respectively.

2.2 Experimental methods

A metallographic specimen with the size of 10 mm × 10 mm × 24.5 mm was obtained from the H62/Q235B clad plate through wire electrical discharge machining (see the cross section in Fig. 1). After polished, the H62 flyer plate was etched with ferric nitrate corrosion solution (5 g $FeNO_3$, 25 ml HCl, and 75 ml H_2O), while the Q235B base plate was etched with 4 % nitric acid alcohol. Then, the bonding interface of the clad plate was observed using a metallographic microscope, and the microstructure and components of it were analyzed using a scanning electron microscope (SEM) and an energy dispersive spectrometer (EDS). Finally, the microhardness in the zone of the bonding interface was measured under the effect of 100 gf of load force for 15 s.

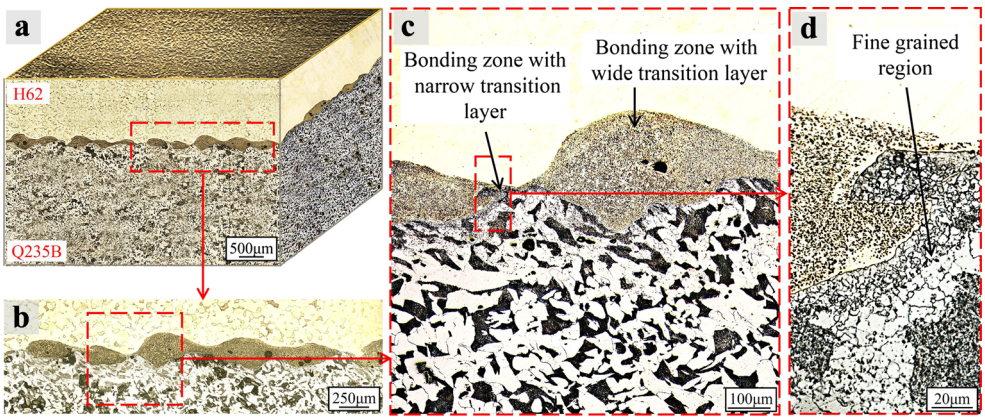

Fig. 4 Optical microstructure observed on the cross section of H62/Q235B clad plate

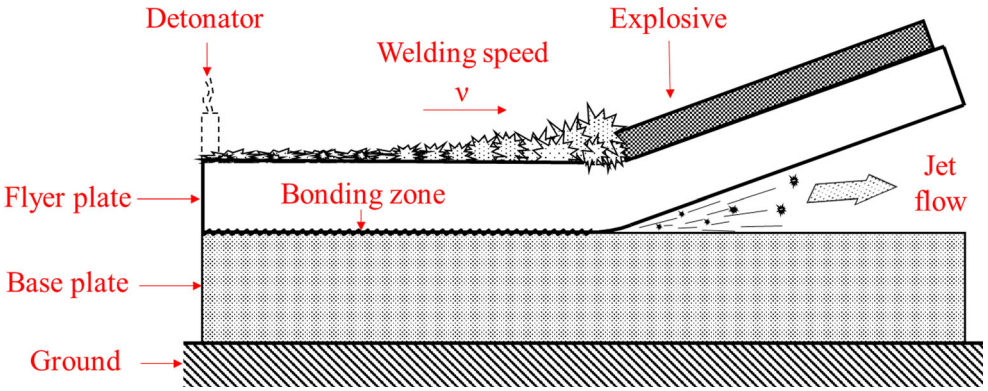

Fig. 5 Schematic of explosive cladding technology

To measure the bonding strength of the H62/Q235B clad plate, the specimens for shear test were machined through wire electrical discharge machining, as illustrated in Fig. 2. Then, shear test was conducted in a universal mechanical testing machine using specialized clamping fixture. After the test, the morphology of the shear fractures was analyzed through SEM observation.

After the external surfaces of the flyer plate and base plate were removed, the specimen for tensile test was sliced layer by layer through wire electrical discharge machining on the premise that the layer containing explosive bonding interface can be obtained. The specimen was then numbered as layers 1–7# from brass to steel. The specific size and sampling plan are shown in Fig. 3. Afterwards, the tensile property of the stratified specimens was tested using the universal mechanical testing machine. Meanwhile, the morphology of the tensile fractures was analyzed through SEM observation.

3 Experimental results and discussion

3.1 Microstructure and components of the bonding interface of the clad plate

Figure 4 which shows the microstructure of the bonding interface of the H62/Q235B clad plate indicates that the bonding interface of this clad plate was periodical wavy. Meanwhile, the bonding interface presented two kinds of typical morphologies, i.e., one was the wide transition layer with a width up to 280 μm and the other was the narrow transition layer with a width less than 20 μm. About 92 % of the total length of the bonding interface consisted of the former, while the latter occupied approximately 8 % of the bonding interface. The wavelength and amplitude for the waves of the bonding interface with a wide transition layer on transversal section were approximately 320–960 μm and 50–280 μm, respectively, whereas 70–140 μm and less than 20 μm, respectively, at the bonding interface with a narrow transition layer.

Figure 5 displays the schematic of explosive cladding process. In this process, detonation waves generated by the explosion of explosives pushed the flyer plate to collide the base plate at a high speed up to several hundreds of meters per second. During this course, most kinetic energy was transformed to thermal energy so that the metals around the impact point were partially melted. These melted metals mixed with unfused ones formed a jet under the huge effect of shock waves to exhaust the air between the two plates in an instant. The metal jet was erupted at a high speed along the forward direction of detonation waves and therefore washed the metal surface of unbonded regions. As a consequence, fresh and clean metals were exposed, thus cleaning the surface. Under the joint action of metal jet and impact pressure, the surfaces of the two metal plates were plastically deformed under high temperature and pressure. Therefore, a periodical wavy bonding interface was formed between the two plates. As the jet can be easily held back in the trough of the base plate, it was cooled and solidified in the local areas and formed the bonding interface through a wide transition layer, while bonding interface with a narrow transition layer was formed in the peak of the base plate as it is difficult to retain the jet there.

As can be seen in Fig. 4b, c, voids were found in partial bonding interface. They were formed owing to the fact that the air between the two plates was wrapped in the transition layer which was rapidly solidified at the moment of explosive cladding. An observation of Fig. 4c, d showed that the grains of the base plate near the bonding interface were obviously refined. This was because the metals near the bonding interface suffered from severe plastic deformation in the process of explosive cladding. As a result, the original microstructure was recrystallized, thus refining the microstructure in this

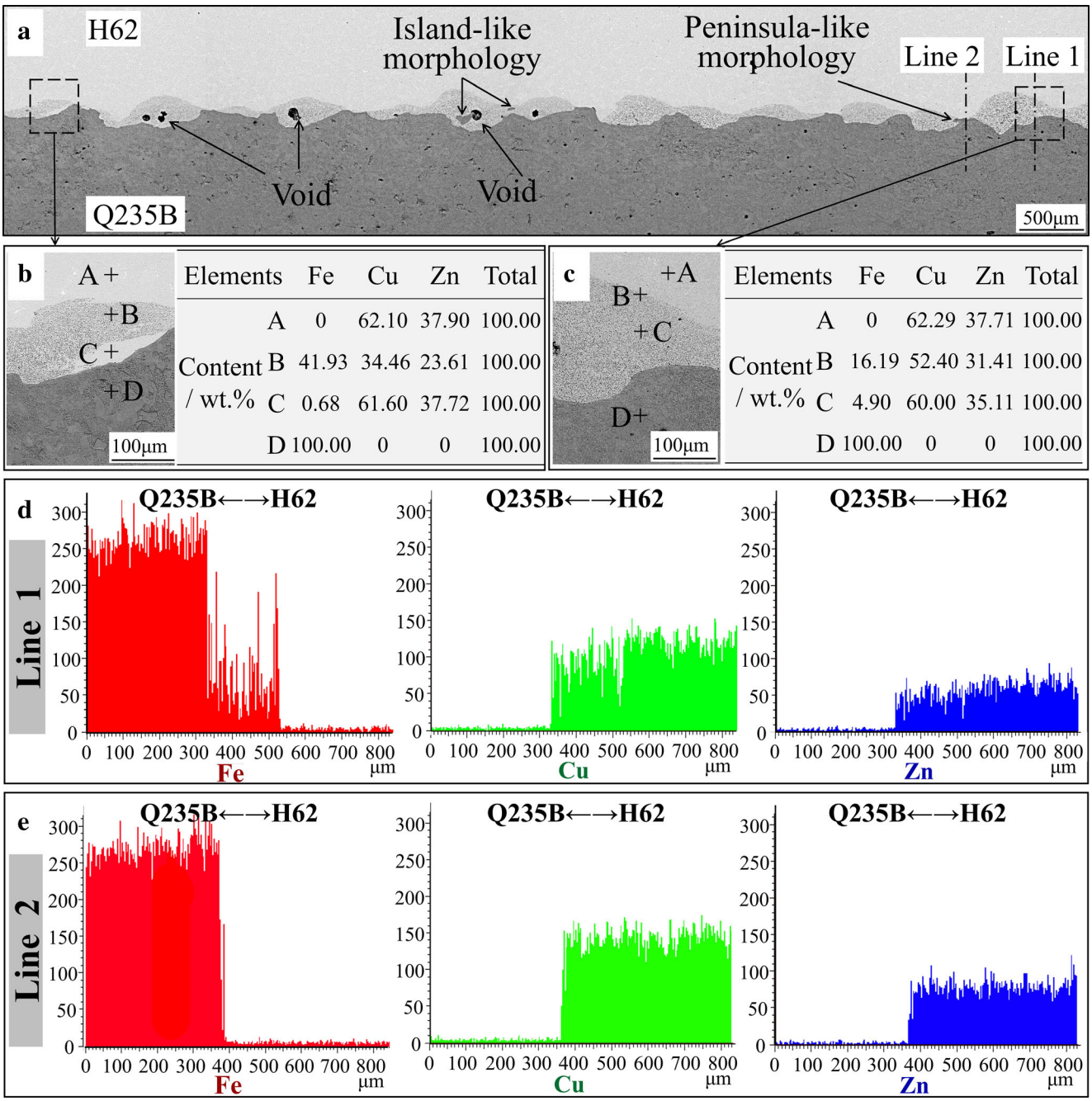

Fig. 6 SEM images and the distribution of elements of the interface in the H62/Q235B clad plate

region. The plastic deformation presented the highest temperature on the bonding interface and the influence of plastic deformation and temperature gradually weakened in the area away from the bonding interface. Therefore, the fineness of grains gradually became lower from the region near the bonding interface to the inner base metal.

The earlier researchers [3, 15, 32] reported that fly lines or adiabatic shear bands were observed near the joint interface in their studies, but there existed no obvious fly lines or adiabatic shear bands in the region near the bonding interface of the H62/Q235B clad plate.

The microstructure and chemical components of the bonding interface were further analyzed using the SEM and EDS and the obtained results were demonstrated in Fig. 6.

The SEM observation (Fig. 6a) illustrated that voids and island-like base metal areas were found in partial

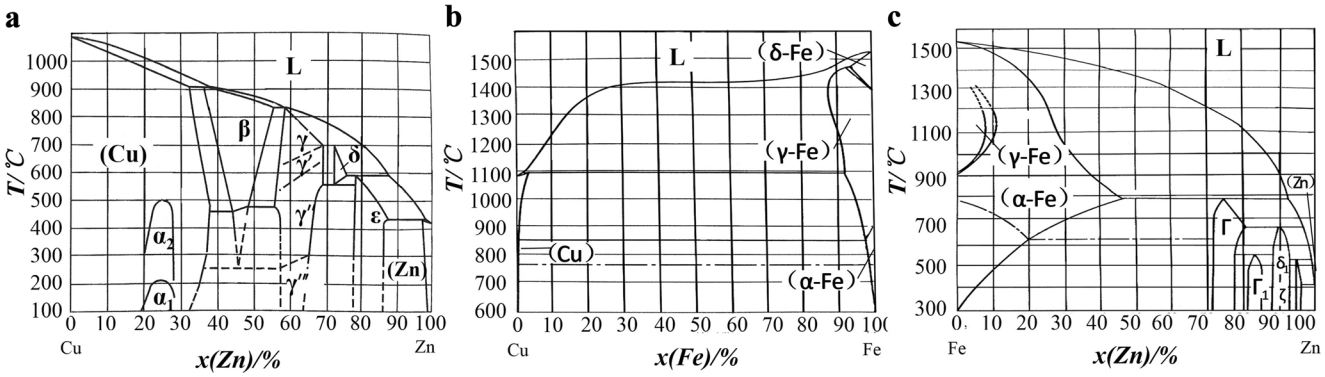

Fig. 7 Binary phase diagrams of **a** Cu-Zn; **b** Cu-Fe; and **c** Fe-Zn [37]

bonding interface, and a majority of the peaks of the base plate were found to be the bonding interface with the narrow transition layer of which the thickness less than 20 μm. The EDS analysis results in Fig. 6b–d showed that the bonding interface of the transition layer contained elements Cu, Zn, and Fe. The former two accounted for a large total proportion, while the latter held a small proportion. This was because the melting point of H62-brass was about 930 °C, while that of Q235B-steel was about 1490 °C. Therefore, a large amount of brass was melted in the explosive cladding, while little steel was fused. Although these three elements showed unstable proportions in the transition layer, the relative ratio of Cu to Zn was basically the same with that of Cu to Zn in the H62-brass.

By combining the binary phase diagrams of Cu-Zn, Cu-Fe, and Fe-Zn in Fig. 7, it was known that when Fe held a small proportion, Fe would dissolve into α-Cu (Zn) to form α-Cu (Zn, Fe) supersaturated solid solutions; when it accounted for a large amount, Cu and Zn would dissolve into γ-Fe (C) to generate γ-Fe (C, Cu, Zn) solid solutions, which would turn into α-Fe (C, Cu, Zn) supersaturated solid solutions when they were rapidly cooled. As the center of the transition layer was cooled slowly, Fe_3C would be separated out in this area.

For the bonding interface with narrow transition layer (Fig. 6e), the compositions of elements suddenly changed in the bonding interface. This is because at the moment of explosive cladding, fresh and clean metal surface was exposed on the bonding interface under the scouring of the metal jet. Under the effect of high temperature and pressure generated by detonation, a thin transition layer was formed between the two metal surfaces. Unapparent diffusion phenomenon occurred to the elements in both sides of the bonding interface at a short distance.

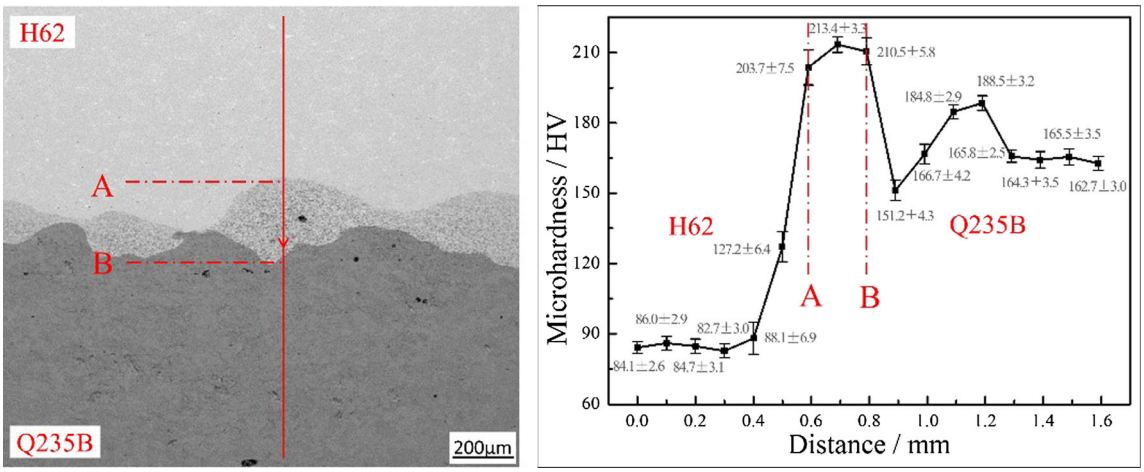

Fig. 8 Microhardness profile across the interface in the H62/Q235B clad plate

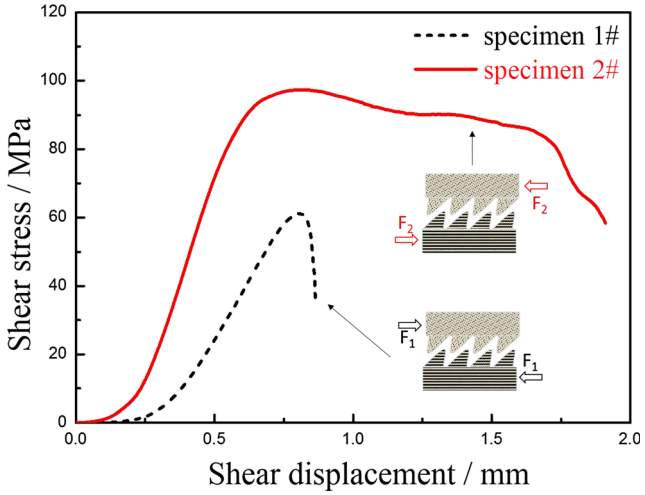

Fig. 9 Shear stress-displacement curves acquired from the shear tests

3.2 Microhardness of the bonding interface of the H62/Q235B clad plate

The micro Vickers hardness was measured for the typical region selected in the bonding interface. Fifty-one measurements from 17 points (3 measurements from each point) were taken from the flyer plate to the base plate, as shown in Fig. 8. As can be seen, the microhardness of the H62-brass and the Q235B-steel far away from the interface was 85 and 165 HV on average, respectively. While the base metals of H62-brass and Q235B-steel adjacent to the transition layer showed the microhardness values of around 203.7 and 210.5 HV, separately. The microhardness at the measured position in the transition layer reached up to approximately 213.4 HV. In the light of the analysis of Fig. 6 above, the main structural components in the transition layer were α-Cu (Zn, Fe), α-Fe (C, Cu, Zn) supersaturated solid solutions, and Fe_3C. Owing to the existence ofthese hard phases, the hardness of the transition layer was obviously higher than that of the base metals.

The microhardness of Q235B-steel was found to reduce firstly and then rise up before finally decreased to the average hardness of the base metal from the side near the transition layer to the inner base metal. On the one hand, the region near the transition layer was recrystallized owing to severe plastic deformation under the impact of explosive and grains therefore were fined (Fig. 4d). Meanwhile, severe plastic deformation also significantly improved the dislocation density of this region [38, 39]. Therefore, obvious work hardening phenomena happened in this region, giving risexto higher microhardness than that of the base metal. On the other hand, the region close to the interface was also subjected to the annealing effect of explosive cladding heat and therefore partial work hardening phenomena were eliminated in the region adjacent to bonding interface, thus reducing the microhardness in the annealing region [40].

3.3 Shear test

Figure 9 shows the typical shear stress-displacement curves obtained from the shear tests. Since the bonding interface was periodical wavy, the shear stress measured was essentially the nominal bonding strength of the interface of the clad plate. As can be seen, the maximal nominal shear stress of the specimen 1# was merely 61.2 MPa and it rapidly reduced after yielding, showing a small shear displacement less than 1 mm. While the specimen 2# showed the maximal nominal shear stress of 97.4 MPa, the plastic deformation lasted for a long plateau stage with the shear displacement being twice that of the specimen 1#.

The morphologies and element distribution of the shear fractures are shown in Fig. 10. As can be seen, the macroscopic shear fractures presented periodical morphologies which were composed of alternative flanges and grooves. By combining Fig. 4, these flanges corresponded to the bonding interface with narrow transition layer, while grooves represented the bonding interface with wide transition layer. That is, the H62/Q235B clad plate was cracked along the explosive wavy bonding interface when it was sheared. Component analysis indicated that the fractures were primarily composed of Cu and Zn, along with little or no Fe. This suggested that the clad plate was stripped along the soft wavy bonding interface in the shear test, that is, the side near the brass. By observing the microstructure of the fractures, the grooves primarily presented lamellar cleavage fractures, showing that this region (bonding interface through wide transition layer) was weakly bonded. A large number of dimples were distributed in the flange region, revealing that this region (bonding interface with narrow transition layer) was well bonded. In addition, no obvious wavy morphologies were found in the right part of the fractures in the specimen 2#, while there were a large amount of dimples and tearing ridges, showing more significant ductile fractures.

Xie et al. [11] also observed the anisotropy of shear property of explosive welded clad plates. They conducted shear tests under the conditions that the angles between shear direction and detonation direction were 0°, 45°, and 90°, respectively. The results showed that the bonding joint exhibited the maximum shear strength when the angle was 90°, while the minimum shear strength was observed when the angle was 0°. However, they made no

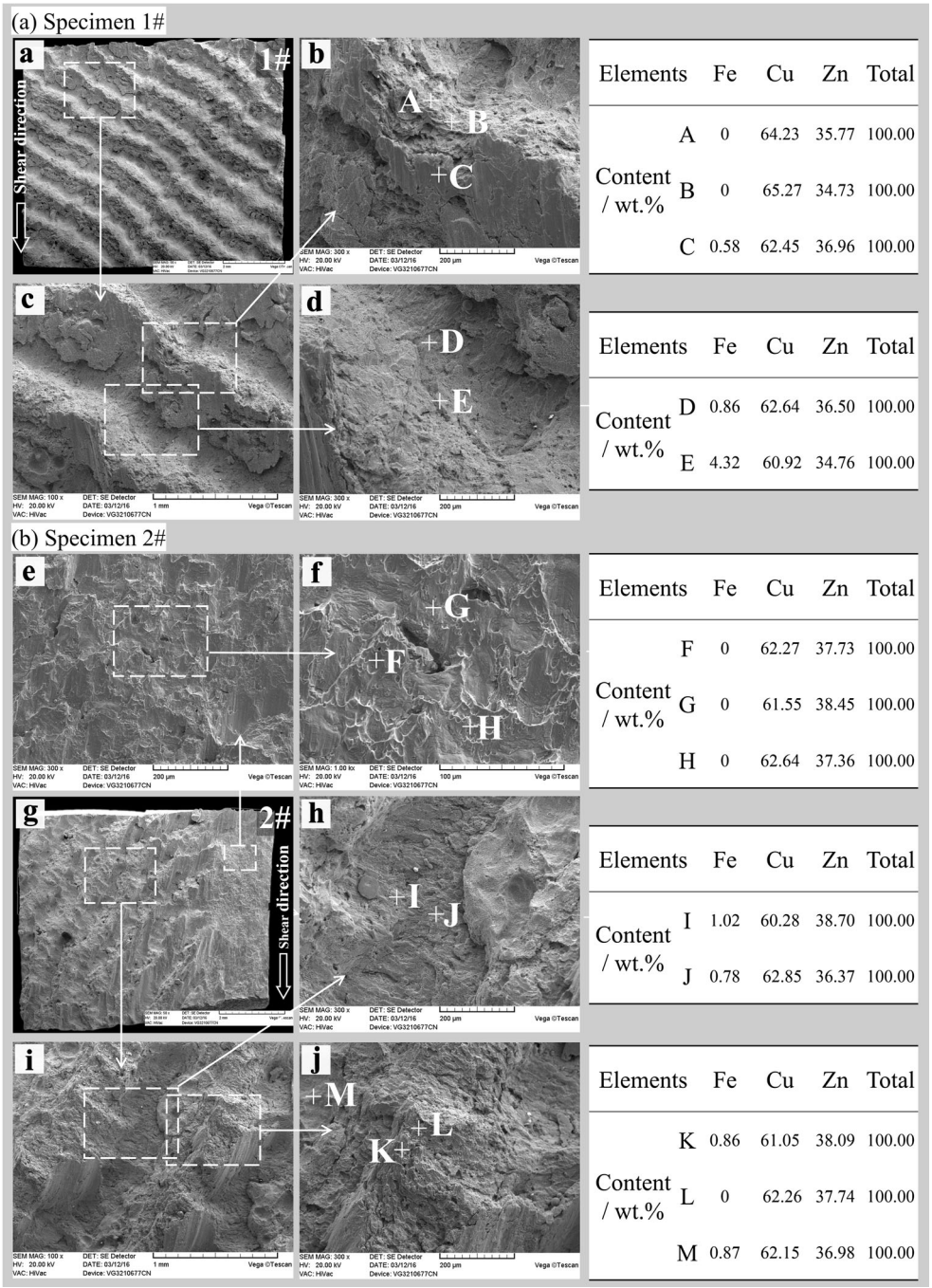

Fig. 10 Morphologies and element distribution of the shear fractures

further analysis on the underlying mechanisms of this phenomenon.

Figure 11 is given here to illustrate how the relative angle between the shear load direction and the detonation wave direction influence the results of shear tests. According to the cross sections of shear fractures in Fig. 11a, b as well as Fig. 6a, the waves in the bonding interface of the H62/Q235B explosive clad plate were basically jagged, especially in the side of the base plate. The bonding status of the up and down waves was shown in Fig. 11c, that was, the waves in the flyer plate and base plate showed opposite forward directions and therefore they were interlocked. Figure 11a illustrates that the shear direction formed a positive angle with the detonation of waves. That is, it acted along the direction of detonation waves, represented by the shear direction of F1 in Fig. 11c. Under such condition, separation of the upper waves and lower waves was subjected to small resistance so that the specimen 1# showed low shear strength. Figure 11b demonstrates that the

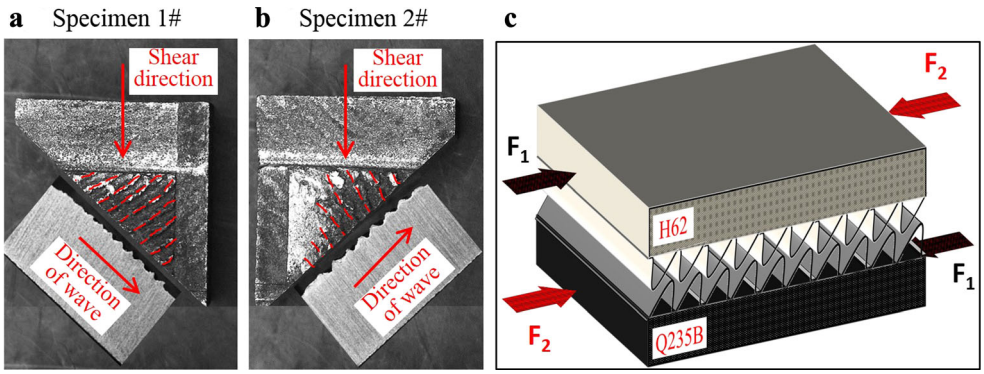

Fig. 11 Schematic of the relationship between directions of shearing and the waves

shear direction for the specimen 2# formed a negative angle with the direction of detonation waves, that was, opposite to the direction of detonation waves (represented by the shear direction of F2 in Fig. 11c). In this case, the peaks of those waves were scratched and the separation of upper waves and lower waves suffered from large resistance. The wave peaks of the metal in the side of soft bonding interface were even completely cut by those in the hard side (the right part of the specimen 2# fracture in Fig. 10b). Therefore, the specimen 2# showed higher shear strength.

3.4 Stratified tensile test

The macroscopic morphologies of the specimens before and after the stratified tensile test were shown in Figure 12a, while the stress-displacement curves of the H62/Q235B clad plate from the stratified tensile test were demonstrated in Fig. 12b. As demonstrated in the figures, after H62-brass (layers 1–3#) was fractured, they showed large elongation and their tensile strength was 355 MPa on average. However, the elongation of Q235B-steel (layers 5–7#) was smaller and the average tensile strength was 503 MPa. In addition, the explosive bonding interface (layer 4#) of the H62/Q235B clad plate showed similar elongation to that of Q235B-steel after being fractured, while its tensile strength (377 MPa) was slightly higher than that of H62-brass.

Based on the observation of the macroscopic morphologies of the fractures of these layers after the stratified tensile test, it was found that the bonding interface (layer 4#) showed different fracture surfaces to those of the base metals of brass (layers 1–3#) and steel (layers 5–7#). Its tensile fractures formed an angle of 45° with the tensile direction. This is because in the stretching process, the layer was cracked at weak positions at first. As the stretching continued, cracks gradually extended. Owing to the discontinuity of the deformation of the metals in both sides of the bonding interface and the low nominal shear strength of the bonding layer, cracks extended along the direction of the maximal shear stress (45°) until the layer was broken.

After the stratified tensile tests, the tensile fractures of layers 1# (H62-brass), 7# (Q235B-steel), and 4# (bonding interface) were observed using the SEM. The acquired

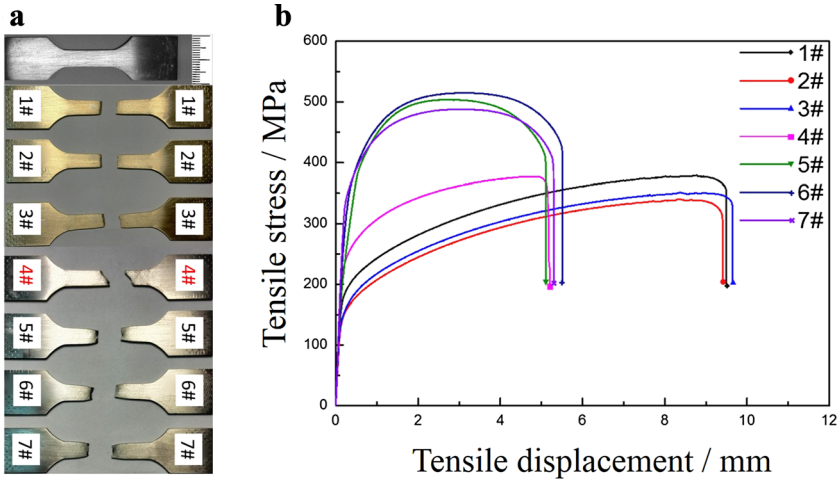

Fig. 12 **a** Morphologies of the specimens and **b** the stress-displacement curves acquired from the stratified tensile tests

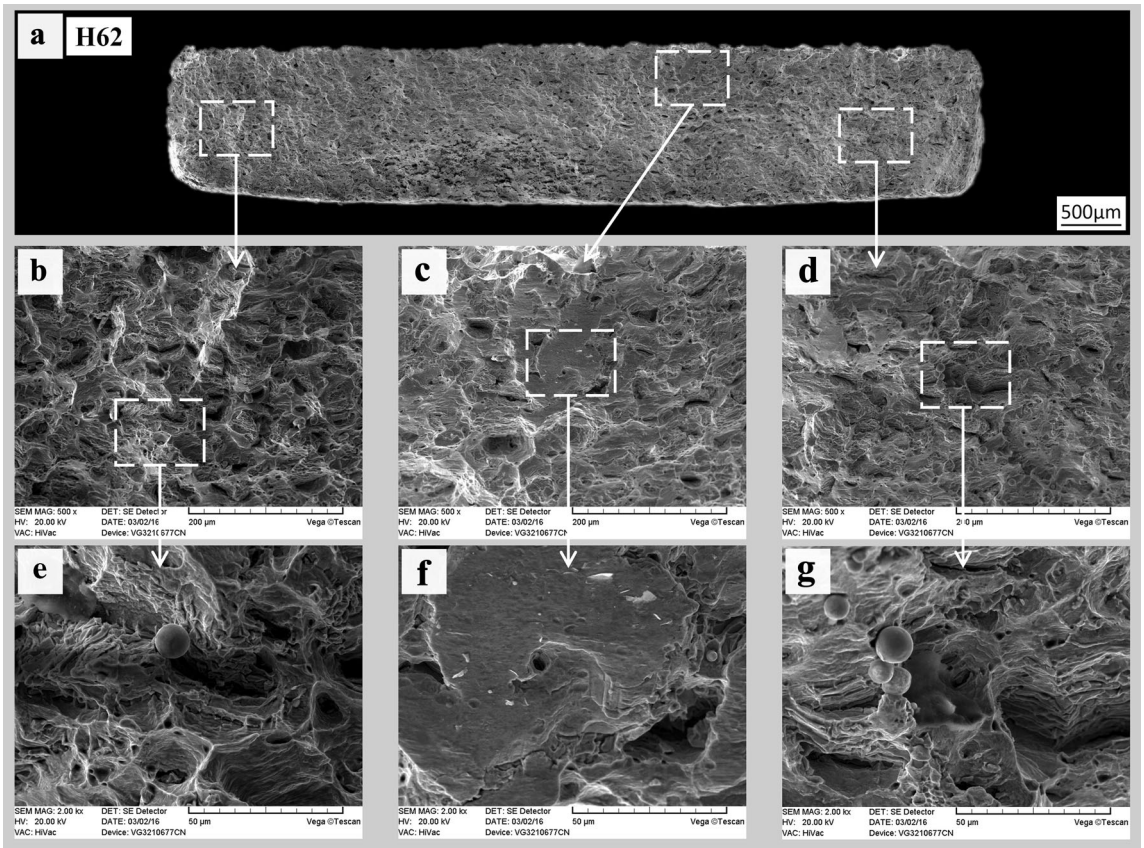

Fig. 13 Fractography of the layer 1# (*H62*) after the tensile test

morphologies of the fractures are demonstrated in Figs. 13, 14, and 15.

According to Fig. 13, the tensile fractures of H62-brass were composed of a large number of ductile fractures and few quasi-cleavage fractures. The fractography primarily consisted of cleavages and shallow dimples. This is because H62-brass is a two-phase brass, that is, α and β' brass at room temperature. Thereinto, α brass is tough and strong, while β' brass is hard and brittle and merely exists in local regions. Therefore, when H62 was stretched, cleavage fractures merely occurred in partial positions. On the whole, the brass still presented ductile fractures which were composed of small dimples [41].

Based on Fig. 14, the tensile fractures of Q235B-steel were typical ductile ones and the fractography was composed of deep and large dimples. Second-phase precipitates were also observed in some dimples.

By comparing Fig. 13 with Fig. 14, the cross section of the fracture of brass was found to be larger than that of steel, showing that the reduction of cross-sectional area of H62 was smaller than that of Q235B-steel.

In accordance with Fig. 15, after the bonding interface of the H62/Q235B clad plate was broken, the fractures of H62-brass were mainly composed of few cleavages and numerous dimples, while deep dimples were the main components of the fractures of Q235B-steel. The flyer plate was basically separated from the base plate along the wavy bonding interface and almost all the transition layers between them were peeled off. The analysis of Fig. 6 showed that there were a large number of supersaturated solid solutions in the transition layers. Owing to the notable inhomogeneity of the microstructure demonstrated in Fig. 4 and Fig. 6, the mechanical property of explosive welded H62-brass/Q235B-steel clad plate changed sharply at the vicinity of bonding interface. As clearly shown in Fig. 8 and Fig. 12, the yield strength and hardness of H62-brass were both lower than that of Q235B-steel; meanwhile, the transition layer which was sandwiched between H62-brass and Q235B-steel was composed primarily of hard supersaturated solid solution, so when the clad plate was stretched, the plastic strain near the H62/Q235B interface was inhomogeneous, and the transition layer could hardly balance the different strain on its both sides. With the increase of tensile load, the mismatch of plastic strain at the boding interface became more and more serious, as well as the stress concentration

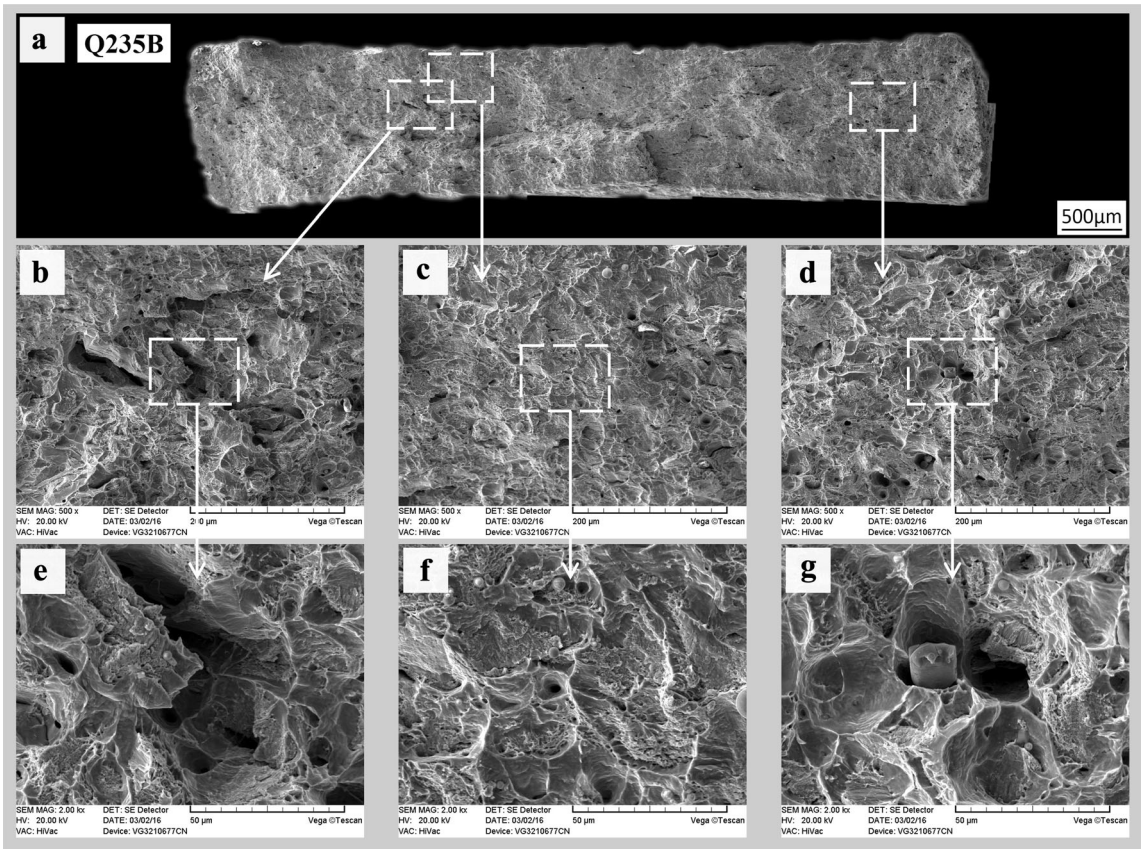

Fig. 14 Fractography of the layer 7# (*Q235B*) after the tensile test

at the bonding interface, especially at the H62-brass/solid-solution interface. As a result, the clad plate was cracked along the bonding interface in the stretching process when the tensile stress was great enough, and most of the fracture existed in flyer plate, as shown in Fig. 10.

4 Conclusions

In order to provide the essential data for the reprocessing of H62/Q235B explosive clad plates, this study investigated the inhomogeneity of the components, microstructure, and mechanical properties of H62/Q235B clad plates. The following conclusions were drawn.

1. The bonding interface of the H62/Q235B explosive clad plate was periodical wavy. The two plates were connected in two ways, that is, through wide transition layers and narrow transition layer, respectively. About 92 % of the total length of the bonding interface consisted of the former, while the latter only occupied approximately 8 % of the bonding interface.
2. The major structural components in the transition layer were α-Cu (Zn, Fe) and α-Fe (C, Cu, Zn) supersaturated solid solutions and Fe_3C.
3. The average microhardness values of the base metals of H62 and Q235B in the regions far away from the interface were 85 and 165 HV, separately. The transition layer showed higher microhardness about 213.3 HV. In the region near the transition layer, owing to the dual action of force and heat, the microhardness of the base plate reduced firstly, then increased and finally decreased again from the interface to the inner base metals.
4. When being sheared, the bonding interface cracked along the transition layer in the side near the brass. The fractures were periodical wavy with flanges and grooves distributed. The shear strength showed an obvious anisotropy. When the plate was sheared along the detonating direction, the shear strength was about 61.2 MPa, while the shear strength was found to be 97.4 MPa when the plate was sheared along the opposite direction, which was 59.2 % higher than the former.
5. Since the reduction of area of H62-brass was smaller than that of Q235B-steel, the tensile fractures

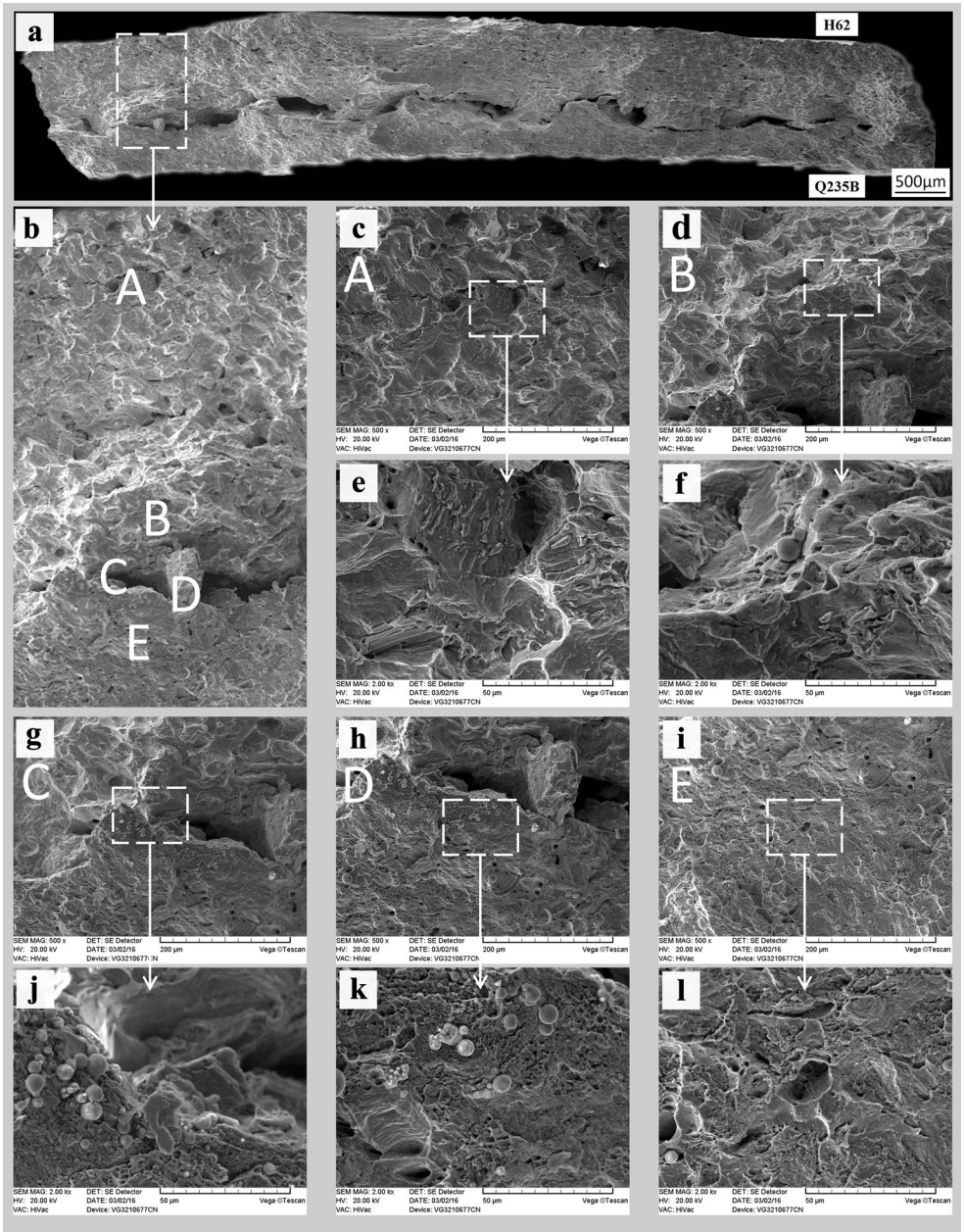

Fig. 15 Fractography of the layer 4# (the bonding interface) after the tensile test

were macroscopically inclined with an angle of 45° owing to the discontinuity of the deformation. The bonding layer was cracked along the wavy bonding interface. Under this condition, the tensile strength was found between those of the base metals of H62-brass and Q235B-steel. The fractography was mainly represented by ductile fractures.

Acknowledgments This work is supported by National High Technology Research and Development Program of China (Grant No. 2013AA031303HZ).

References

1. Li L, Zhou DJ (2016) Investigation and application of Al clad steel materials. Metal World 1:15–20
2. Gou NN, Zhang JX, Zhang LJ, Li ZG, Bi ZY (2016) Single pass fiber laser butt welding of explosively welded 2205/X65 bimetallic sheets and study on the properties of the welded joint. Int J Adv Manuf Tech:1–11
3. Malyutina YN, Skorohod KA, Shevtsova KE, Chesnokova AV (2015) Multilayered titanium-steel composite produced by explosive welding. AIP Conf Proc 1683(1):20142–113123
4. Kahraman N, Gülenç B, Findik F (2005) Joining of titanium/stainless steel by explosive welding and effect on interface. J Mater Process Tech 169(2):127–133

5. Raghukandan K (2003) Analysis of the explosive cladding of Cu-low carbon steel plates. J Mater Process Tech 139: 573–577
6. Wang XX, Wang JX, Zhao Z, He Y (2014) Parameters of the interfacial waves of Zr/steel composite plate by explosive welding. Rare Metal Mat Eng 43(3):682–685
7. Manikandan P, Lee JO, Mizumachi K, Mori A, Raghukandan K, Hokamoto K (2011) Underwater explosive welding of thin tungsten foils and copper. J Nucl Mater 418(1):281–285
8. Findik F (2011) Recent developments in explosive welding. Mater Design 32(3):1081–1093
9. Kacar R, Acarer M (2004) An investigation on the explosive cladding of 316L stainless steel-din-P355GH steel. J Mater Process Tech 152(1):91–96
10. Kahraman N, Gülenç B, Findik F (2007) Corrosion and mechanical-microstructural aspects of dissimilar joints of Ti-6Al-4V and Al plates. Int J Impact Eng 34(8):1423–1432
11. Xie MX, Zhang LJ, Zhang GF, Zhang JX, Bi ZY, Li PC (2015) Microstructure and mechanical properties of CP-Ti/X65 bimetallic sheets fabricated by explosive welding and hot rolling. Mater Design 87:181–197
12. Bataev IA, Bataev AA, Mali VI, Pavliukova DV (2012) Structural and mechanical properties of metallic–intermetallic laminate composites produced by explosive welding and annealing. Mater Design 35:225–234
13. Acarer M, Gulenc B, Findik F (2003) Investigation of explosive welding parameters and their effects on microhardness and shear strength. Mater Design 24(8):659–664
14. Heidarzadeh A, Jabbari M, Esmaily M (2015) Prediction of grain size and mechanical properties in friction stir welded pure copper joints using a thermal model. Int J Adv Manuf Tech 77(9-12): 1819–1829
15. Zhang LJ, Ning J, Zhang XJ, Zhang GF, Zhang JX (2015) Single pass hybrid laser-MIG welding of 4 mm thick copper without preheating. Mater Design 74:1–18
16. Poovannan A (2015) Optimization of ultrasonic metal welding parameters for copper sheet to copper wire joints and numerical analysis of ultrasonic wire bonding. Int J Appl Eng Res 10(2):3301–3310
17. Zhang GF, Takahashi Y, Heng Z (2015) Ultrasonic weldability of Al ribbon to Cu sheet and the dissimilar joint formation mode. Mater Trans 56(11):1842–1851
18. Ning J, Zhang LJ, Wang A, Bai QL, Yang JN, Zhang JX (2016) Effects of double-pass welding and extrusion on mechanical properties of fiber laser welded 1.5-mm thick T2 copper joints. J Mater Process Tech 237:75–87
19. Li Y, Hu S, Shen J, Liu L (2015) Microstructures and mechanical properties of H62-brass-316L stainless steel in overlap welded joints by continuous-wave laser. Int J Adv Manuf Tech 79(1-4):627–634
20. Chen HC, Bi G, Nai MLS, Wei J (2015) Enhanced welding efficiency in laser welding of highly reflective pure copper. J Mater Process Tech 216:287–293
21. Zhang LJ, Bai QL, Ning J, Wang A, Yang JN, Yin XQ, Zhang JX (2016) A comparative study on the microstructure and properties of copper joint between MIG welding and laser-MIG hybrid welding. Mater Design 110(15):35–50
22. Schmidt HC, Ebbert C, Rodman D, Homberg W, Grundmeier G, Maier HJ (2015) Investigation of cold pressure welding: cohesion coefficient of copper. Key Eng Mat 651:1421–1426
23. Kanigalpula PKC, Pratihar DK, Jha MN, Derose J, Bapat AV, Rudra Pal A (2015) Experimental investigations, input-output modeling and optimization for electron beam welding of Cu-Cr-Zr alloy plates. Int J Adv Manuf Tech 85(1):711–726
24. Enzinger N, Loidolt P, Wiednig C, Stütz M, Sommitsch C (2016) Electron beam welding of thick-walled copper components. Sci Technol Weld Joi:1–6
25. Zhou L, Zhou WL, Feng JC, He WX, Huang YX, Dong SS (2015) Effect of rotation speed on the microstructure and mechanical properties of dissimilar friction stir-welded copper/brass metals. Int J Adv Manuf Tech 54(6):1–9
26. Zhang GF, Zhang LJ, Kang CW, Zhang JX (2016) Development of friction stir spot brazing (FSSB). Mater Design 94:502–514
27. Farrokhi H, Heidarzadeh A, Saeid T (2013) Frictions stir welding of copper under different welding parameters and media. Sci Technol Weld Joi 18(8):697–702
28. Pashazadeh H, Teimournezhad J, Masoumi A (2016) Experimental investigation on material flow and mechanical properties in friction stir welding of copper sheets. Int J Adv Manuf Tech:1–10.
29. Mróz S, Szota P, Stefanik A, Wąsek S, Stradomski G (2015) Analysis of Al-Cu bimetallic bars properties after explosive welding and rolling in modified passes. Arch Metal Mater 60(1): 427–432
30. Durgutlu A, Gülenç B, Findik F (2005) Examination of copper/stainless steel joints formed by explosive welding. Mater Design 26(6):497–507
31. Xue ZG, Huang XL, Gao BL (2016) Technology research on the large area Cu/steel clad plate with explosive welding. Dev Appl Mater 31(1):41–44
32. Zhai WG, Wang SG, Luo CX, Ding F (2013) Microstructure and mechanical properties of Cu-steel composite plate with explosive welding. Weld Join 4:35–40
33. Bian C, Wang FY, Yang XB, Shen ZX, Wan TQ (2016) Feasibility study on explosive welding of copper and high nitrogen steel composite panel. Hot Work Tech 45(5):222–226
34. Qu YD, Zhang WJ, Kong XQ, Zhao X (2016) Theoretical investigation of calculating temperatures in the combining zone of Cu/Fe composite plate jointed by explosive welding. Phys Met Metallogr+ 117(3):260–266
35. Li HF, Duan WD (2005) Manufacture of the copper/steel kelmet scaleboard with the method of explosive welding. Blasting 22(3): 101–104
36. Liu YC, Di JH, Wang ZS, Zhang BM (2003) The study on bonding mechanism of explosive welding of A3 steel and brass. J North Univ China 24(2):94–97
37. Li JH (2009) The metallographic phases of metals. China Machine Press, Beijing
38. Loureiro A, Mendes R, Ribeiro JB, Leal RM, Galvão I (2016) Effect of explosive mixture on quality of explosive welds of copper to aluminium. Mater Design 95:256–267
39. Acarer M, Gülenç B, Findik F (2004) The influence of some factors on steel/steel bonding quality on the characteristics of explosive welding joints. J Mater Sci 39(21):6457–6466
40. Guo XZ, Tao J, Yuan Z, Zhang L, Sun X (2012) Interface and properties of explosive welded TA1/Al clad tube. Rare Metal Mat Eng 41(1):139–142
41. Shi CG, Wang Y, You J (2007) New achievements on the theory and technology of explosive welding. Explos Mater 36(3):27–30